

Phosphorus cluster production by laser ablation

A.V. Bulgakov* and O.F. Bobrenok
*Institute of Thermophysics SB RAS,
 1 Lavrentyev Ave., 630090 Novosibirsk, Russia*

I. Ozerov,[†] W. Marine, and S. Giorgio
*CRMC-N, UPR 7251 CNRS, Université de la Méditerranée,
 Faculté des Sciences de Luminy, Case 901,
 13288 Marseille Cedex 9, France*

A. Lassesson and E.E.B. Campbell
*School of Physics and Engineering Physics,
 Göteborg University and Chalmers University of Technology,
 SE-41296, Göteborg, Sweden*

Neutral and charged phosphorus clusters of a wide size range have been produced by pulsed laser ablation (PLA) in vacuum at 532, 337, and 193 nm ablating wavelengths and investigated by time-of-flight mass spectrometry. The neutral P_n clusters are even-numbered with local abundance maxima at $n = 10$ and 14 , while the cationic and anionic clusters are preferentially odd-numbered with P_7^+ , P_{21}^+ , and P_{17}^- being the most abundant ions. The dominance of the magic clusters is more pronounced at 337-nm ablation that is explained by efficient direct ejection of their building blocks under these conditions. Nanocrystalline phosphorus films have been produced by PLA in ambient helium gas.

PACS numbers: 52.38.MF; 61.46.+w; 79.20.Ds; 81.07.B; 81.16.Mk

One of the greatest potentials of pulsed laser ablation (PLA) is in the development of novel nanoscale materials. Recently there has been renewed interest in the study of phosphorus clusters and nanostructures as potential candidates to form fullerene-like and nanotubular materials [1, 2, 3, 4]. Elemental phosphorus has been obtained in more allotropic modifications than any other element [5] and one would thus expect a variety of structural forms of P_n clusters. Phosphorus clusters have been studied extensively in the last decade by theoretical approaches focused mainly on two structural families, cages (polyhedra) and chains [3, 4, 5, 6, 7, 8, 9, 10, 11, 12, 13]. A number of structures for P_n clusters ($n > 4$) have been proposed as energetically more stable than tetrahedral P_4 . Also, the viability of phosphorus nanotubes has been predicted [1].

The theoretical suggestions, however, are still not confirmed by experiment. The observed dominance of P_4 in phosphorus vapor and apparent instability of larger clusters provided a puzzle for several decades [6]. Only a few experiments have been performed on clusters larger than P_4 [9, 11, 14, 15]. Recently, a wide spectrum of neutral and cationic phosphorus clusters were synthesized by visible PLA [2]. Different cluster distributions were observed under far-UV PLA resulting in stable hydride phosphorus clusters [16].

In this work we continue our investigations on phos-

phorus cluster production by PLA. Three different ablation regimes, at 532 nm, 337 nm, and 193 nm laser wavelengths, have been studied and compared with respect to P_n cluster generation. Mechanisms of cluster formation under PLA conditions are discussed. In addition, the first attempt to produce nanocluster phosphorus films by PLA technique has been performed.

I. EXPERIMENT

The apparatus used for laser ablation and cluster production and detection was described earlier [2, 16, 17]. The target (crystalline red phosphorus of 99.999% purity with respect to metals) was placed in a rotating holder in a vacuum chamber (base pressure 10^{-5} Pa) and irradiated by a ns laser pulse. Three different laser systems operating at 337 nm (10 ns pulse, N_2 laser), 532 nm (13 ns, Nd:YAG laser, 2nd harmonic), and 193 nm (15 ns, ArF laser) were used for ablation. The laser fluence at the target was varied in the range 20 – 800 mJ/cm² for each wavelength. The relative abundance of neutral and charged particles in the PLA plume was analyzed by time-of-flight (TOF) mass spectrometry. The plume expanded under field-free conditions over a distance of 6 cm (at 532-nm ablation) or 7 cm (at 337 and 193-nm ablations) towards a repeller grid where the plume ions were sampled by pulsing the grid at a time delay t after the laser pulse. Electron-impact ionization (90 eV) and a plasma suppressor were used to investigate neutrals [2]. Every mass spectrum was summed over 200 laser shots.

*Electronic address: bulgakov@itp.nsc.ru

[†]Electronic address: ozerov@crmcn.univ-mrs.fr

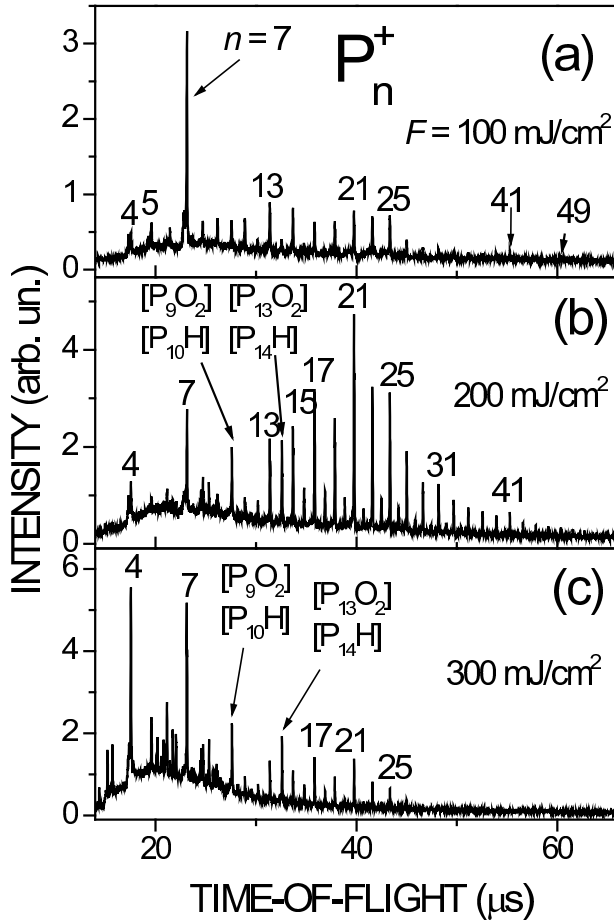


FIG. 1: Mass spectra of cationic phosphorus clusters produced by 337-nm laser ablation at time delay $t = 62 \mu\text{s}$ for three different laser fluences.

The nanostructured phosphorus films were deposited on fused silica substrates using 193-nm PLA both in vacuum and in an ambient gas. In the latter case, a continuous flux of pure helium was introduced into the chamber at a pressure of 400 Pa. The ArF laser fluence was set at 650 mJ/cm^2 . The substrates were placed at a distance of 5 cm from the target and kept at either room or liquid nitrogen (LN) temperature. The films were characterized by transmission electron microscopy (TEM) and by electron diffraction (ED) using a Jeol 2000FX microscope.

II. RESULTS AND DISCUSSION

With the 532 nm and 337 nm ablating wavelengths, neutral phosphorus clusters P_n of a wide size range (up to $n = 40$), their cations P_n^+ (up to $n = 91$), and anions P_n^- (up to $n = 49$) have been produced in abundance in the PLA plume. Figure 1 shows the TOF mass spectra of the cationic species at 337-nm ablation for three different laser fluences. The mass spectra were taken at

an "optimum" delay time t corresponding to maximum yield of P_n clusters with $n > 9$. An interesting feature of the mass spectra is the strong fluence dependence for generation of large phosphorus clusters that dominate in the plume at a narrow fluence range around 200 mJ/cm^2 but represent only minor constituents at 100 and 300 mJ/cm^2 . In contrast, smaller P_n clusters ($n < 9$) are observed in a much larger fluence range and their concentration increases progressively with fluence.

Another interesting feature of the cation mass spectra shown in Fig. 1 is the distinct odd-even alternation with domination of odd-numbered clusters and local maxima at $n = 17, 21, 25, 31, 41$, and 49 . Under the "optimum" conditions, P_{21}^+ is remarkably prominent with its peak intensity at least a factor of 2 larger than that of other clusters (Fig. 1b). It should be noted here that direct comparison of intensities of small and large clusters is difficult because of the inherent decline in detector response at high masses. For fairly large clusters, the detection efficiency decreases as the particle impact velocity decreases down to a threshold value of $\sim 20 \text{ km/s}$ [18]. For the present experiments, the ion impact energy was 5 keV and thus clusters with masses above roughly 2500 u (i.e., at $n > 80$ for P_n clusters) were detected with significantly decreasing efficiency. In the lower mass range, however, the detector response is a rather weak function of impact velocity as was confirmed by a calibration of our microchannel plate detector with a C_{60} ion beam. For instance, the detection efficiencies for two magic clusters P_{21}^+ and P_{41}^+ differ by a factor of ~ 1.4 whereas their experimental intensities differ by an order of magnitude. Thus, the observed abundance distribution is expected to give a good indication of the true one.

Even-numbered P_n^+ clusters are present in minor amounts up to $n = 40$ (Fig. 1) as double peaks separated by 1 u. The second, stronger, peak in the bunch is attributed to either $P_n\text{H}^+$ or $P_{n-1}\text{O}_2^+$ ($n = \text{even}$) which could not be distinguished in our experiment. Both H and O atoms come from trace impurities in the target as was confirmed by laser desorption MS analysis. The relative abundance of the compound clusters increases with fluence (Fig. 1c). It has already been speculated that a dodecahedral cage-like P_{20} , stabilized with an additional fourfold coordinated P atom in the laser plasma, could be especially stable and explain the magic number of 21 [2]. The energetic stability of the dodecahedral structure for neutral P_{20} was recently confirmed by calculations [4, 13]. A similar cation mass spectrum as shown in Fig. 1b was obtained with a 532-nm ablating wavelength at an "optimum" laser fluence of around 300 mJ/cm^2 [2]. However, the 337-nm ablation resulted in a higher abundance of large P_n^+ clusters and in a more pronounced preference of the P_{21}^+ magic cluster. Further reduction in laser wavelength down to 193 nm resulted again in a lower abundance of bare P_n clusters and in generation of compound clusters with the $P_{23}\text{H}_6^+$ cation being the most stable [16].

To further elucidate the cluster formation process, the

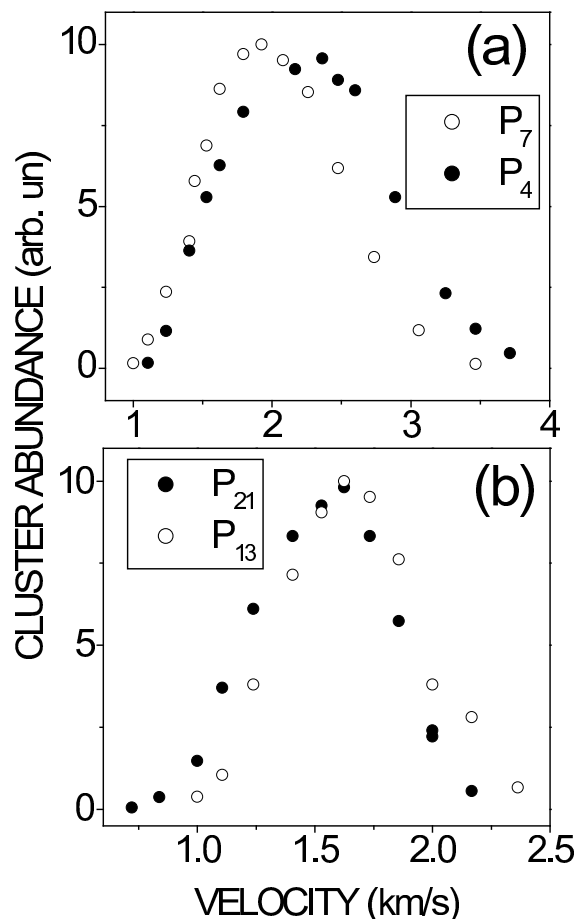


FIG. 2: Velocity distributions for small (a) and large (b) phosphorus cluster cations produced by 532-nm laser ablation at 300 mJ/cm^2 .

plume dynamics has been examined by varying the time delay t . Figure 2 illustrates typical velocity distributions for several representative clusters obtained at 532-nm ablation under "optimum" conditions. A clearly different expansion behavior is seen for small ($n < 9$) and larger species. The large P_n clusters have near equal expansion velocities ($\sim 1.6 \text{ km/s}$ for these conditions, Fig. 2b) over a wide size range in spite of the large difference in their masses. This implies a gas-phase condensation mechanism for their formation rather than direct ejection [2, 16]. Smaller P_n clusters have size-dependent velocities ($\sim 2 \text{ km/s}$ for P_7^+ and $\sim 2.4 \text{ km/s}$ for P_4^+ , Fig. 2a) and appear to be ejected from the target. A plausible explanation for the efficient generation of large phosphorus clusters by PLA without a carrier gas is, therefore, that their building blocks (small P_n clusters) have been already formed in the target and ejected thus facilitating the gas-phase cluster growth. It is important that the building blocks are larger than P_4 in order to avoid simple polymerization of P_4 during the clustering process

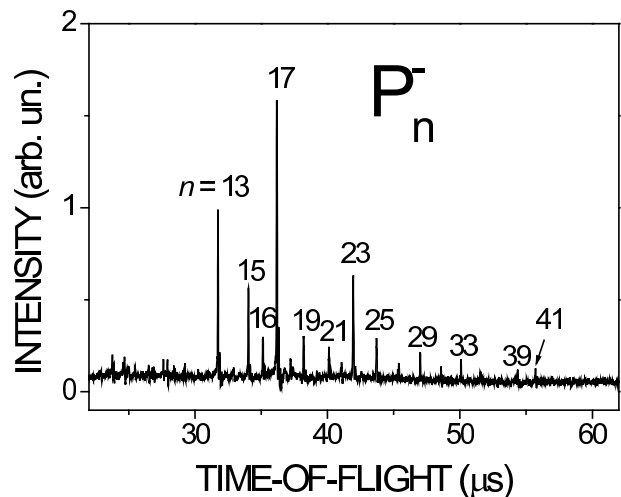


FIG. 3: Mass spectrum of anionic phosphorus clusters produced by 337-nm laser ablation at $t = 62 \mu\text{s}$ and $F = 200 \text{ mJ/cm}^2$.

[6].

The highest abundance of large P_n^+ clusters observed under 337-nm ablation indicates that this regime appears to be around the most favorable one for emission of their building blocks via a non-thermal mechanism. An additional evidence for the direct cluster ejection is that the relatively large species ($n > 4$) were observed at very low threshold fluences (around 100 mJ/cm^2 for 532 nm and 50 mJ/cm^2 for 337 nm) when no smaller fragments were detected. Longer laser wavelengths result in a higher contribution of the thermal vaporization mechanism and thus in higher abundance of atoms and small P_n molecules ($n < 5$) among the vaporized products [5, 16]. On the other hand, for far-UV laser ablation, ejection of the intact building blocks is less efficient due to their subsequent photodissociation and more efficient photoionization of the target impurities promotes formation of the compound clusters [16].

Along with the P_n^+ cations, anionic and neutral phosphorus clusters of a wide size range are also abundant in the plume. Figure 3 shows a mass spectrum of P_n^- anions produced under the same conditions as for Fig. 1b. Again a pronounced odd-even alternation is observed with preferred formation of odd-numbered clusters. However, the magic numbers are essentially different from those for P_n^+ clusters. At $n > 23$, a four-fold periodicity for anionic magic numbers is evident. The strongest peak corresponds to P_{17}^- . At $n > 10$, P_{16}^- and P_{18}^- anions are the only observed even-numbered bare clusters. A similar anion distribution was observed at 532-nm ablation [15], again with less pronounced magic clusters. The difference in abundance distributions for anionic and cationic phosphorus clusters suggests that their stable structures are different as well. Indeed, recent calculations for small P_n clusters (up to $n = 9$) showed that the cluster geom-

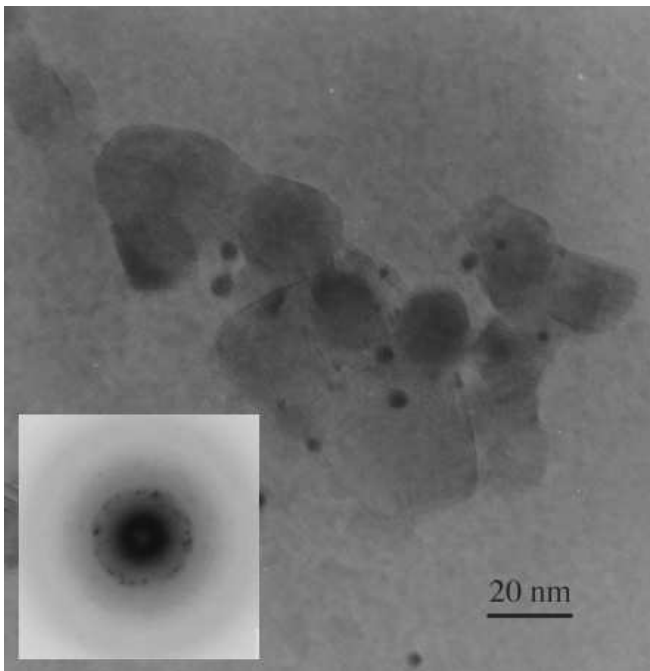


FIG. 4: TEM image of nanocrystalline phosphorus film produced by 193-nm laser ablation in 400 Pa helium. The inset shows the corresponding ED pattern.

etry changed considerably when the degree of charging was changed [3].

In contrast to the ionized species, neutral P_n clusters are even-numbered [2, 16]. The magic clusters are observed at $n = 10$ and 14 that correspond to the local maxima for the compound cationic clusters at high fluences (Fig 1c). A local abundance minimum at $n = 22$ indicates the presence of polyhedral P_n in the PLA plume [2]. The comparison of the absolute yields for neutral and charged clusters is not straightforward since the electron impact ionization efficiency for P_n clusters is unknown. Assuming the average cluster ionization cross-section to be $2 \times 10^{-15} \text{ cm}^2$ (maximum value for P_4 [19]), we have found that the concentration of neutral P_n clusters is at least an order of magnitude higher than for the corresponding P_{n+1} cations. Furthermore, the distribution of the neutrals could be distorted by ionization-induced fragmentation. We expect, however, that this has only a minor effect in our case since, at least for small P_n clusters, dissociative ionization is a considerably less efficient process than electron impact direct ionization [19].

In spite of the relatively efficient generation of P_n clusters under PLA in vacuum, the produced clusters are still fairly small and present in the plume in a marginal quan-

tity. In order to synthesize a large quantity of nanoclusters we performed PLA in a helium atmosphere. The role of the ambient gas is to confine the laser ablation plume thus favoring gas-phase condensation during the collisional stage of plume expansion. The initial small clusters act as nucleation centers for the cluster growth. Figure 4 shows a TEM image of a sample deposited on a substrate at LN temperature. The film consists of near-spherical clusters with an average size of about 20 nm and has an intense orange color. Some smaller clusters with mean size of 3 nm are also present in the film. The electron diffraction pattern (inset in Fig. 4) corresponds to a crystalline material with the spacing between atomic planes of 2.8 ± 0.15 , 2.1 and 1.8 Å. The complex diffraction pattern corresponds to the coexistence of several different structures of red phosphorus [5]. Films deposited at room temperature are composed of nanocrystals with larger sizes, probably due to their aggregation and coalescence on the substrate. In contrast to the crystalline films obtained in the helium atmosphere, nanostructured films deposited in vacuum from small phosphorus clusters were amorphous. We suggest that the high kinetic energy of the species arriving on the substrate results in cluster melting followed by a rapid cooling without crystallization.

III. CONCLUSIONS

Neutral and charged phosphorus clusters have been produced by visible (532 nm) and near-UV (337 nm) PLA under vacuum conditions in narrow laser fluence ranges centered at around 200 and 300 mJ/cm² for 337 and 532 nm, respectively. A series of magic clusters, particularly neutral P_{10} and P_{14} , cationic P_7^+ and P_{21}^+ , and anionic P_{17}^- have been observed. Preferences of the magic clusters are more pronounced at 337-nm PLA that is explained by efficient direct ejection of their building blocks (small P_n clusters with $n < 9$) under these conditions. Nanocrystalline phosphorus films have been deposited by PLA in an ambient gas atmosphere. The crystallites have a mean size of about 20 nm and their crystalline structure corresponds to that of red phosphorus.

Acknowledgments

This work was partly supported by the Russian Foundation for Basic Research (Grant No. 02-03-32221a) and the Royal Swedish Academy of Science (KVA).

[1] G. Seifert, E. Hernández: Chem. Phys. Lett. **318**, 355 (2000)
 [2] A.V. Bulgakov, O.F. Bobrenok, V.I. Kosyakov: Chem.

Phys. Lett. **320**, 19 (2000)
 [3] M.D. Chen, R.B. Huang, L.S. Zheng, Q.E. Zhang, C.T.Au: Chem. Phys. Lett. **325**, 22 (2000)

- [4] G. Seifert, T. Heine, P.W. Fowler: *Eur. Phys. J. D* **16**, 341 (2001)
- [5] D.E.C. Corbridge: *The Structural Chemistry of Phosphorus*, Elsevier, Amsterdam, 1974
- [6] R.O. Jones, D. Hohl: *J. Chem. Phys.* **92**, 6710 (1990)
- [7] R.O. Jones, G. Seifert: *J. Chem. Phys.* **96**, 7564 (1992)
- [8] M. Häser, U. Schneider, R. Ahlrichs: *J. Am. Chem. Soc.* **114**, 9551 (1992)
- [9] R.O. Jones, G. Ganteför, S. Hunsicker, P. Pieperrhoff: *J. Chem. Phys.* **103**, 9549 (1995)
- [10] M. Häser, O. Treutler: *J. Chem. Phys.* **102**, 3703 (1995)
- [11] R. Huang, H. Li, Z. Lin, S. Yang: *J. Phys. Chem.* **99**, 1418 (1995)
- [12] M.D. Chen, J.T. Li, R.B. Huang, L.S. Zheng, C.T. Au: *Chem. Phys. Lett.* **305**, 439 (1999)
- [13] B. Song, P.-l. Cao: *Phys. Lett. A* **291**, 343 (2001)
- [14] T.P. Martin: *Z. Phys. D* **3**, 211 (1986)
- [15] Z. Liu, R. Huang, L. Zheng: *Z. Phys. D* **38**, 171 (1996)
- [16] A.V. Bulgakov, O.F. Bobrenok, V.I. Kosyakov, I. Ozerov, W. Marine, M. Hedén, F. Rohmund, E.E.B. Campbell: *Phys. Solid State* **44**, 617 (2002)
- [17] L. Patrone, D. Nelson, V.I. Safarov, S. Giorgio, M. Sentis, W. Marine: *Appl. Phys. A* **69**[Suppl.], S217 (1999)
- [18] R.J. Buehler, L. Friedman: *Nucl. Instrum. Methods* **170**, 309 (1980)
- [19] G. Monnom, Ph. Gaucherel, C. Paparoditis: *J. Phys.* **45**, 77 (1984)